RSC Advances

PAPER

View Article Online
View Journal | View Issue

Cite this: *RSC Adv.*, 2025, **15**, 8645

Investigating the wettability of neem oil nanoemulsion as a green pesticide on leaf surfaces – optimizing formulation, assessing stability, and enhancing wettability†

Jayita Chopra, * Priyanka Sahoo, Pradeep Kumar Sow and Vivek Rangarajan

The present study focuses on formulating a stable green oil-in-water nanoemulsion (NE) formulation for pesticide application, thereby addressing the primary challenges of botanical pesticides by improving the stability, efficacy, and wettability of leaf surfaces. Neem oil and rhamnolipid biosurfactant were utilized as the base oil and surfactant, respectively for the NE formulation. Initial screening studies with varying oil-to-surfactant ratios identified an optimal ratio of 7.13 (w/w), corresponding to 15% oil (v/v) of total emulsion volume, for a stable NE. The stability of the formulation was validated in a 25 mL volume over 20 days, maintaining a mean droplet diameter of 139.1 ± 7.34 nm and a polydispersity index of 0.207. Further stability assessments under varying time, temperature, ionic strengths, and centrifugal forces revealed a relatively stable droplet diameter ranging from 141 to 245 nm. The surface tension for the optimal formulation was measured to be 35.7 ± 0.4 mN m^{-1}. Additionally, experiments with various NE formulations on selected leaves showed that NEs with higher oil content displayed faster spreading, as indicated by a rapid reduction in contact angle. The novelty of the study lies in demonstrating the synergistic interaction between oil and rhamnolipid, which facilitated faster spreading compared to the individual spreading of either component, as revealed by the dynamic spreading studies of the NE formulation on leaf surfaces. Therefore, this research paves the way for future research and development of green pesticides that are sustainable and effective compared to their chemical counterparts.

Received 23rd January 2025
Accepted 12th March 2025

DOI: 10.1039/d5ra00556f

rsc.li/rsc-advances

1 Introduction

Pesticides encompass a wide array of synthetic compounds employed to control pest infestations in plants. Nevertheless, the pervasive use of these chemical agents has elicited considerable concern due to their detrimental impact on ecosystems. Many of these pesticides, particularly organophosphates, undergo biomagnification within food chains, posing significant threats to higher trophic levels.[1] Furthermore, the hydrophobic nature of most conventional pesticides limits their effective deployment to targeted areas. Consequently, fostering sustainable agricultural practices necessitates a shift away from reliance on chemical pesticides toward the adoption of bio-based alternatives that offer more uniform distribution patterns. Emulsifiable concentrates are the most commonly employed for hydrophobic pesticides, and they often rely on organic solvents, which pose hazards such as flammability, explosiveness, human toxicity, and significant environmental impact. Microemulsions are one of the promising alternatives to emulsifiable concentrates. However, the challenges include limiting loading capacity, *i.e.*, incorporating pesticides at a higher level. Also, more than one type of surfactant is required for microemulsion formulations.[2]

Nanoemulsions (NEs) can overcome most of the problems associated with emulsifiable concentrate and microemulsions. NEs are composed of submicron-sized uniform droplets ranging from 20 to 200 nm and have emerged as a promising colloidal dispersion with significant stability attributed to micellar formation through the interaction of oil and surfactant.[3] The inherent stability of NEs, resistant to gravitational separation, flocculation, and coalescence-induced creaming underscores their potential applications.[4] The smaller size of NE ensures higher deposition, diffusion, and permeability on plant surfaces thereby enhancing pesticide bioavailability and leaf surface wettability, categorizing them as fungicides, herbicides, or insecticides based on target organisms. Even though NEs are deemed thermodynamically unstable due to their proneness to spontaneous phase separation, if micellar attractions diminish over time when exposed to external stress

Department of Chemical Engineering, BITS Pilani K K Birla Goa Campus, Goa, India. E-mail: jayitac@goa.bits-pilani.ac.in

† Electronic supplementary information (ESI) available. See DOI: https://doi.org/10.1039/d5ra00556f

factors, exemplified by Ostwald ripening, they can still have good kinetic stability.[5]

Embodying an oil phase dispersed in water (O/W) through the aid of surfactants, NEs are prepared using high-energy (ultrasonication and high-speed homogenization) or low-energy (phase inversion) emulsification methods.[3] Despite the energy-intensive nature of this emulsification process (~108 W kg^{-1}), it yields more uniform-sized droplets (~100 nm) with prolonged stability, making it the method of choice for the current study. A combination of collision, compression, and cavitation helps to overcome the interfacial tension between the oil and water phases.[6] NE prepared by sonication is easily scalable with low production costs.

Augmenting NE stability involves the addition of an appropriate biosurfactant at an optimum dose, where the surfactant's type and composition critically influence NE stability.[7] The selection of an appropriate surfactant is paramount in synthesizing stable NEs, tailored to specific applications. Beyond conventional synthetic options, a range of eco-friendly surfactants exists, including biopolymer-based variants such as proteins (*e.g.*, whey, casein), polysaccharides (*e.g.*, glycolipids), and natural compounds (*e.g.*, saponin, gum arabic). Drawing from prior investigations conducted by our research team, Ganesan *et al.*, (2023),[7] rhamnolipid emerges as a promising green surfactant for NE synthesis. Rhamnolipids, classified as glycolipids, can be produced through fermentation utilizing the *Pseudomonas aeruginosa* strain. Rhamnolipids typically consist of one or two polar rhamnose units covalently linked to a non-polar fatty acid chain, incorporating a hydroxylalkanoate moiety. The hydrophilic head group of rhamnolipids features a carboxylic acid group, rendering them anionic under specific pH conditions. The fatty acid chain length usually varies from C_8–C_{14}.[8] This unique molecular structure confers surface activity upon rhamnolipids due to the simultaneous presence of polar and non-polar regions within the same molecule.[9] Critical micellar concentrations (CMC) are typically 10–200 mg L^{-1}, which is 10–100 times lower than conventional chemical surfactants.[10] The hydrophilic–lipophilic balance (HLB) reported in the literature is around 6.5.[11] Despite their potential, research investigating the formation and stability of emulsions utilizing rhamnolipids remains limited.

Identification of the oil phase is crucial for green pesticide formulation. Using medicinal oil as the oil phase can help overcome the harmful impacts associated with chemical pesticides. Diverse botanical formulations, encompassing plant extracts and essential oils, have undergone rigorous testing, demonstrating efficacy against a broad spectrum of pests.[12,13] Notably, neem oil derived from the *Azadirachta indica* plant has garnered widespread attention due to its rich composition of active compounds, including azadirachtin A, azadirachtin B, salanine, nimbin, among others.[14] The germicidal and antibacterial properties are primarily contributed by the main ingredient, azadirachtin, rendering it effective against a wide range of pests. Moreover, using neem oil in a pesticide formulation presents multiple advantages over traditional chemical pesticides. It effectively tackles issues like pesticide resistance, which arises from the repeated use of the same pesticide, as well as pest resurgence, fostering a more sustainable environmental approach.[15] However, the commercialization of neem oil has faced challenges due to the presence of numerous compounds exhibiting varying degrees of stability and bioactivity. Therefore, developing strategies aimed at enhancing the stability of neem oil formulations stands as a pivotal step towards ensuring efficient and sustainable pest control solutions.

Existing studies on neem oil NEs for pesticide application predominantly employ synthetic surfactants, emphasizing a gap in bio-based formulations.[16] Neem oil NE synthesis with Tween 80 and gum arabic has been reported by Mossa *et al.* (2022)[17] to study insecticidal properties against mosquitoes (Culex sp.). Furthermore, understanding the spreading behavior of NE droplets on leaf surfaces is essential. Presently, there are limited studies examining the wetting behavior of green NEs, particularly concerning the microstructures and roughness of leaf surfaces.

To address the research gap and to formulate a pesticide with all green constituents, the current study aims to optimize NE formulation with rhamnolipid, a biosurfactant, for stable neem oil-NE, encompassing comprehensive characterization, stability tests under stress conditions, and wettability studies on leaf surfaces with varying hydrophobicity and surface roughness. This research endeavor seeks to contribute valuable insights into the development of efficient and sustainable neem-based pest control solutions, bridging the gap between bio-based formulations and practical agricultural applications.

2 Materials and methods

2.1 Chemicals and reagents

Neem oil (100% pure) was purchased from Young Chemist Pvt. Ltd (Gujarat, India). Rhamnolipid (Purity 90% from *Pseudomonas aeruginosa*) was procured from Sigma Aldrich (Mumbai, India). Rose and hibiscus leaves were obtained from the campus garden.

2.2 Formulation of stable emulsion

2.2.1 Screening. The preliminary investigations aimed at determining optimal oil concentration to achieve stable NE involved the use of a compact ultrasonication probe from Qsonica Q500 (Newtown, USA) with a 1/8″ diameter. Screening studies were performed by varying the oil% (5, 10, 15, 20) v/v ratio to obtain the emulsion with a desired diameter having maximum stability. The corresponding oil/surfactant (O/S) ratios were 2.37, 4.75, 7.13 and 9.51 (w/w). The rhamnolipid concentration was maintained at a constant of 16.6 g L^{-1}. These experiments were conducted in 2 mL Eppendorf tubes, utilizing a total emulsion volume of 1.5 mL. Screening studies were carried out with a short duration of 3 minutes, employing a cycle of 5 seconds ON and 10 seconds OFF, at an amplitude of 40% and a consistent frequency of 20 kHz. This standardized approach was applied in the formulation of NE to ensure consistent results during the screening process. The NE synthesis process has been depicted in Fig. 1. The mean droplet size of the generated NEs in all conducted studies was assessed

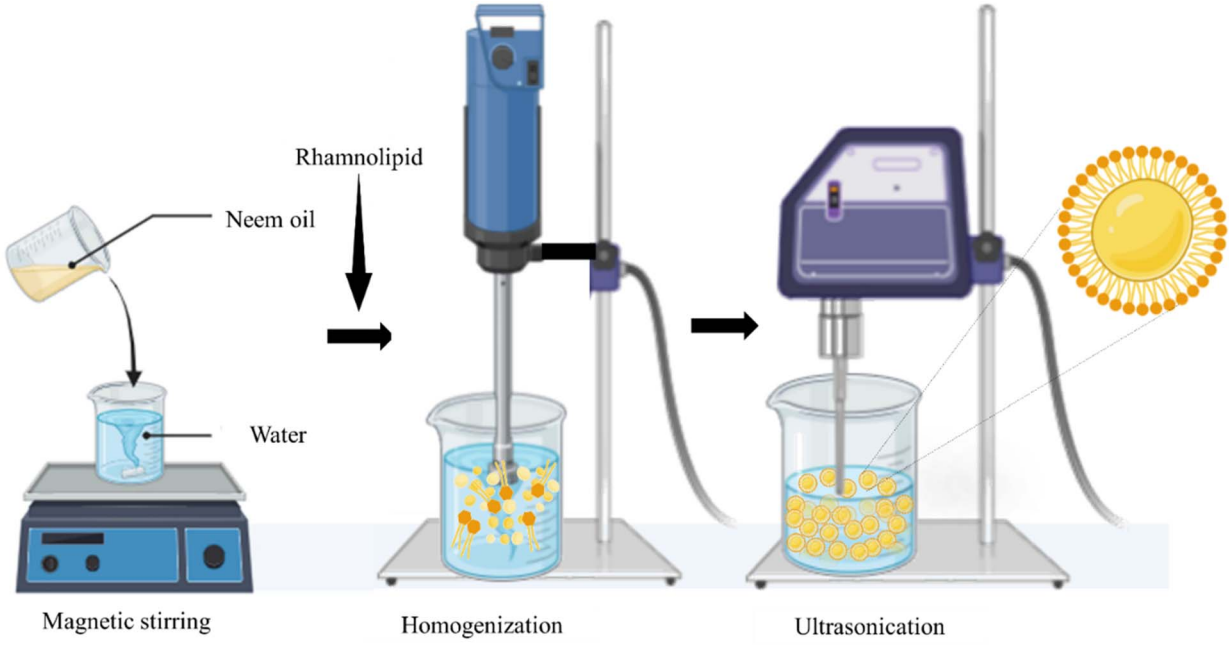

Fig. 1 Schematic of rhamnolipid stabilized neem oil NE synthesis.

through dynamic light scattering analysis (DLS) using Particulate Systems-Nanoplus 3 (Norcross, USA). Subsequently, the concentration of oil yielding a smaller droplet size while maintaining stability without any phase separation over a 30 day testing period, was identified as the optimal concentration. This selected concentration served as the basis for further refinement and optimization studies.

A stability test was performed for a 30 day period to confirm the optimization results. The stability test was aimed at observing any phase separation and creaming behavior. Hydrodynamic diameter (HDD) and polydispersity index (PDI) were measured for the 0th day and the 30th day.

2.2.2 Validation of optimized formulation. Experiments were conducted to confirm the optimal formulation from the screening studies. An ultrasonicator equipped with a 1/2″ diameter probe was utilized, to manage a total emulsion volume of 25 mL. Prior to ultrasonication, all samples underwent pre-emulsification through a high-speed homogenizer, specifically the IKA T10 basic Ultra-Turrax from Berlin, Germany, operating for approximately 3 minutes. All samples were prepared in triplicate, and HDD, PDI and zeta potential were measured for all the samples.

2.2.3 Stability test of NE

2.2.3.1 Time. The stability of the NE, synthesized under optimal conditions, was evaluated by periodically monitoring the dispersed droplet size at 25 °C. This assessment employed DLS method over a testing duration of 30 days.

2.2.3.2 Temperature. The stability of NEs after being exposed to temperatures of 40 °C, 60 °C, 80 °C, and 100 °C was evaluated. The test was performed by keeping freshly prepared NEs in the water bath, at set temperatures for 30 minutes and bringing the samples to 25 °C before analysis for DLS for the measurement of droplet size and PDI.

2.2.3.3 Centrifugation. NE samples of 2 mL volume were subjected to centrifugation at a temperature of 25 °C for 30 min. The stability of the samples was tested for different rotational speeds of 2000, 4000, 6000, 8000, 10 000 and 12 000 rpm corresponding to relative centrifugal force (RCF) of relative centrifugal force (RCF)—650, 2598, 5846, 10 394, 16 240 and 23 386*g*, respectively. Sample analysis was done using DLS analyzer.

2.2.3.4 Ionic strength. To assess the stability of the NE, a 20 μL sample was introduced into 2 mL of NaCl solution with varying concentrations (ranging from 1 g L^{-1} to 75 g L^{-1}), each freshly prepared as stock solutions. Following a 15 minute incubation period, all samples underwent droplet size analysis using DLS. This approach provided a comprehensive evaluation of NE stability under different NaCl concentrations, ensuring a thorough examination of potential changes in droplet size over time.

2.3 Analysis of NE

2.3.1 Droplet size measurement using DLS. The droplet size distribution of the NEs was analyzed utilizing a DLS analyzer, the Particulate Systems Nanoplus 3 (Norcross, USA), operating at a temperature of 25 °C. Approximately 50 μL of the NE sample was dispersed in 2 mL of water within an Eppendorf tube and delicately mixed using a vortex mixer. Crucial parameters such as the HDD and the PDI were recorded for each sample, ensuring comprehensive characterization of the NE's particle size distribution.

2.3.2 Determination of zeta potential. The zeta potential was determined by employing an identical analyzer discussed in the preceding section. However, the cuvette cell was substituted with a flow cell setup for this assessment. The sample's zeta potential was assessed utilizing a 10-fold diluted NE sample

(*i.e.*, 2 mL in 20 mL water), with its value deduced from the electrophoretic mobility of oil droplets. Zeta potential analysis was exclusively conducted on samples of optimal composition. All measurements were performed in triplicate, and the resultant values were presented as the mean of three replicates, ensuring robust and reliable data acquisition.

Microscope images of the emulsion were captured at varying magnifications using a Labomed Model Lx-500 Trino LED microscope.

2.4 Surface tension and wettability studies

The surface tension of the emulsion was measured using the pendant drop method. Contact angle measurements were performed with an Attension Theta surface tensiometer at a controlled temperature of 24 ± 1 °C. A 10 μL droplet of the test solution was manually deposited on the test surfaces for evaluation. The test surfaces included a glass slide, serving as a smooth, non-textured substrate, and leaves from rose and hibiscus plants. The leaves were freshly collected, rinsed with water, and allowed to air dry before use. Contact angles for the NE, surfactant solution, and water were measured on these surfaces. The evolution of the contact angle was recorded over 150 seconds for each sample. The density required for surface tension evaluation was determined by weighing a 1 mL volume of the test liquid using a precision balance (Shimadzu AP225WD). The density was calculated based on this volume measurement and repeated five times to ensure accuracy. The average density value was then used for surface tension evaluation using the pendant drop method. SEM analysis of the leaves was performed using the field emission scanning electron microscope (Quanta FEG-250) under different magnifications.

2.5 Statistical analysis

The values of hydrodynamic diameter (HDD) of the oil droplets and PDI of all nanoemulsion samples were expressed as a mean of three different experiments ±SD. The analyses of variance (ANOVA) were conducted to check the differences between the samples for varying oil-to-surfactant ratios. A value of $p < 0.05$ was considered statistically significant.

3 Results and discussion

3.1 Screening study

The optimal concentration of surfactant ensures the desired particle size, stability, viscosity, and antimicrobial properties of NE necessary for targeted applications. However, the surplus surfactant can lead to toxic effects at excessively high concentrations. Therefore, the screening study aimed to determine the optimal oil-to-surfactant (O/S) ratio for achieving a stable NE formulation, marking a crucial optimization phase in NE synthesis. Fig. 2 illustrates the mean HDD and PDI of various formulations on the day of synthesis (day 0) and after one week. Throughout this period, all NE formulations exhibited visual stability. The HDD values of nanoemulsion samples increased with an increase in oil content ($p < 0.05$), ranging from 199.2 nm to 244.6 nm for O/S of 2.37 and 4.75, respectively. Notably, the formulation with O/S of 7.13 recorded the minimum HDD (194.9 nm on day 0 and 186.8 nm after 1 week) with almost stable PDI (0.218 and 0.225 for 0th day and 1 week, respectively). These findings were corroborated by a visual assessment of stability over one month, which revealed no phase separation for the 4.75 and 7.13 O/S (Fig. 3), indicating their suitability as ideal compositions. Conversely, the O/S of 9.51 formulation exhibited complete separation after 30 days. The droplet size and PDI for different formulations after 30 day period have been included in the ESI (Fig. S2†). A droplet size range of <200 nm is considered suitable for NE for pesticide application as it ensures enhanced dispersion of loaded pesticide. Various reports show stable NE with droplets in the same size range observed in the current study.[18] The optimal concentration (O/S 7.13) had an O/W ratio of 0.13 (w/w), which is similar to that reported for saponin–glycerol stabilized almond oil NE with optimal O/W as 10/90, *i.e.* 0.11 w/w.[19] The density of neem oil, was 789 kg m^{-3}, which was lower than other oils used in

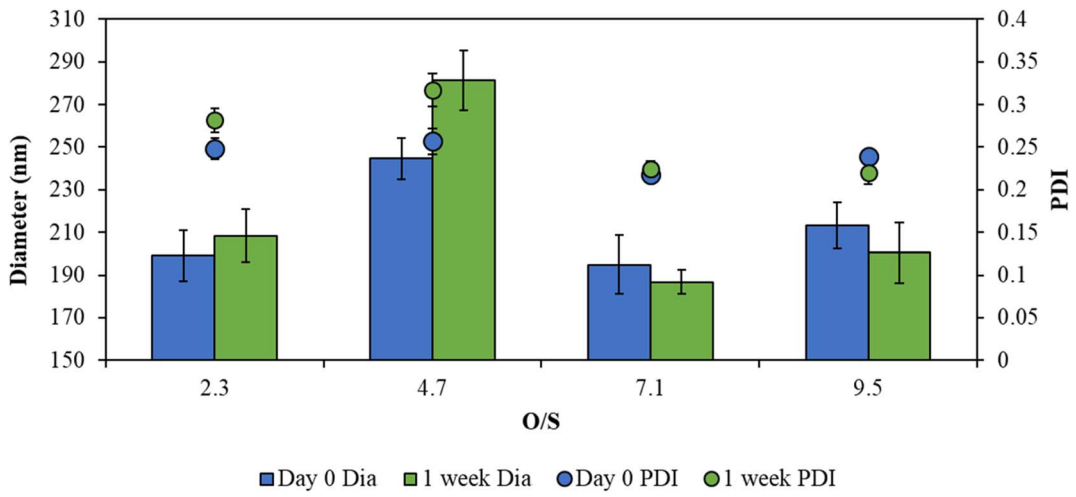

Fig. 2 HDD and PDI of NE formulations with different O/S ratios on the 0th day and after 1 week.

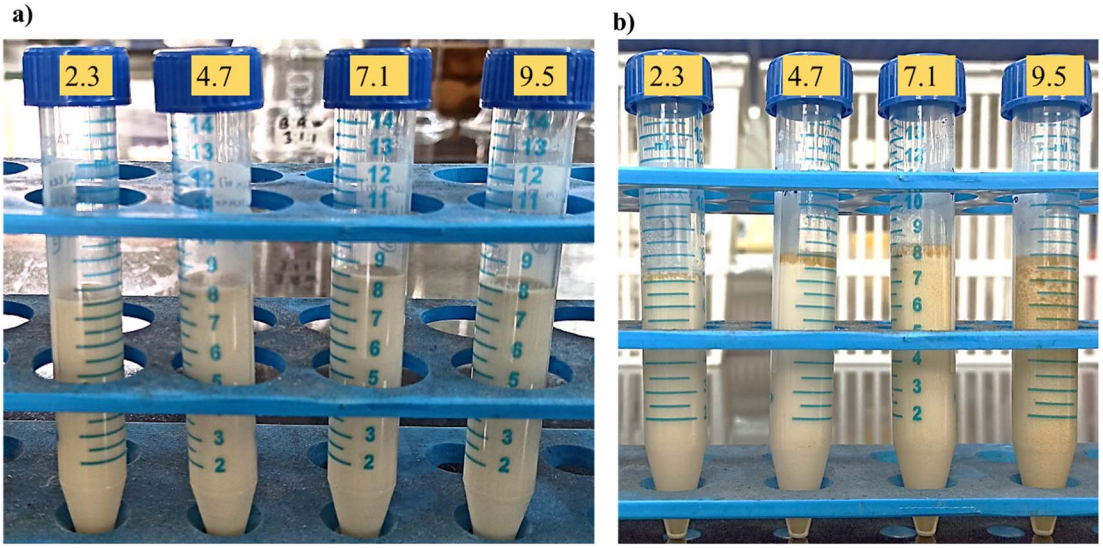

Fig. 3 NE formulations on the (a) 0th day showing no phase separation and (b) after 30 days showing little phase separation in NE with O/S of 4.7 and 7.1 and significant separation in 9.5.

literature for NE synthesis, such as almond oil (913 kg m^{-3}) and peppermint oil (898 kg m^{-3}). The approximate oil% (v/v) for the different formulations varied from 5% to 20% with an optimal of 15% (corresponding to O/S of 7.13). Carpenter and Saharan (2017)[20] observed that at a higher O/S ratio, NEs are destabilized primarily due to the limited availability of surfactants to saturate the oil droplets. A minimal droplet size of 164.7 ± 5.55 nm was observed for eugenol oil-in-water NE stabilized with Tween 80 and Span 80 for an O/S of 1 : 1. The diffusion coefficient of eugenol oil was found to increase with O/S ratio, indicating lower O/S ratios are more stable because it restricts the mobility of oil molecules.[21]

3.2 Validation of optimized formulation

The aforementioned study determined the most effective NE formulation possessing an O/S ratio of 7.1. Subsequently, this formulation was validated in a 25 mL volume NE following the procedure outlined in section 2.2.2. As depicted in Table 1, the HDD, PDI, and zeta potential were measured for samples on both 0th and 20th days. Contrary to the widely established observation that Ostwald ripening typically increases droplet size due to the diffusion of smaller droplets into larger ones, the observed reduction in hydrodynamic diameter (HDD) from 150.36 ± 6.39 nm (day 0) to 139.1 ± 7.34 nm (day 20) suggests an alternative mechanism driving this decrease. One plausible explanation is interfacial stabilization, mediated by the subtle reorientation of the rhamnolipid biosurfactant system at the oil–water interface, likely influenced by its larger head group.[7] Furthermore, the slight reduction in the polydispersity index (PDI) suggests a more uniform droplet size distribution, indicating enhanced system stability and reinforcing the role of interfacial stabilization over Ostwald ripening.[22] The HDD obtained in a larger volume (150.36 ± 6.39 nm for 25 mL) is lesser compared to the HDD obtained for a smaller volume (194.9 ± 13.6 nm for 10 mL) and can be attributed to the variation in energy input in the larger (500 W, 20 kHz) and smaller (125 W, 20 kHz) sonication probe. Zeta potential (ZP) is a measure of the surface charge of droplets in a liquid and is used to predict dispersion stability.[23] In the current study, both samples were found to have sufficiently high negative surface charges. The ZP values were similar to those reported by Dordević *et al.* (2015).[24] NEs are typically deemed stable when their zeta potential values exceed 30 mV, regardless of whether they are positively or negatively charged.[25]

Table 1 Hydrodynamic diameter, polydispersity index and zeta potential of the optimized NE formulation (O/S-7.1)

	HDD[a] (nm)	PDI	Zeta potential (mV)
Day 0	150.36 ± 6.39	0.219 ± 0.01	−45
Day 20	139.1 ± 7.34	0.207 ± 0.01	−47

[a] HDD and PDI values are given as mean ± SD for triplicate. Zeta potential is avg of two values.

3.3 Stability studies

3.3.1 Thermal stability. This investigation examined the impact of storage temperature (ranging from 40 to 100 °C) on NE stability. Throughout the temperature spectrum, minimal variation in HDD and PDI was observed, suggesting robust stability of the NE formulation, as depicted in Fig. 4a. Nevertheless, a slightly bimodal nature of the peak following heat treatment at 100 °C indicates potential future droplet aggregation of varying sizes. This is corroborated by the comparatively elevated PDI value for this specific sample. In a study by Yan *et al.* (2024),[26] the particle size, PDI, and zeta potential were measured at 240, 0.3, and 31 nm, respectively, for NEs coated with octenyl succinic anhydride-modified chitosan and loaded with DHA, subsequent to heat treatment at 60 °C for 30

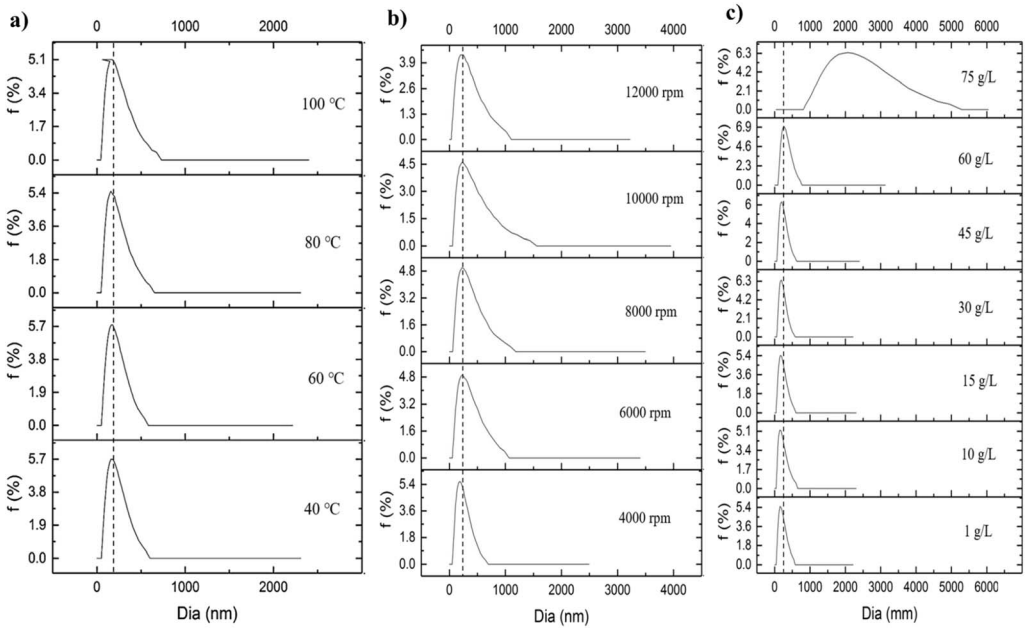

Fig. 4 Differential intensity (*f*%) profile of NE droplets as measured by DLS under varied conditions (a) temperature, (b) centrifugal force and (c) salt concentration.

minutes. Throughout the current study, the NE remained stable, showing no signs of precipitation or aggregation and maintaining its original appearance. PDI value is a crucial parameter in evaluating NE's uniformity, particle dispersion, and stability. An optimal PDI value close to 0 is indicative of exceptional homogeneity and stability within NE formulations.[27] Hence, relatively constant PDI values observed in the current study confirm the uniform distribution of particle sizes. Thermal stability studies are required to assess the stability of NE as a pesticide when exposed to varied temperatures during transportation and storage. Therefore, the neem oil NE formulation can be a potential pesticide option owing to its high thermal stability.

3.3.2 Centrifugal force. The kinetic stability or separation resistance of the NE was tested under various centrifugal forces. As shown in Fig. 4b, centrifugation had minimal impact on the HDD and PDI of the particles. No phase separation or sedimentation was observed even after subjecting the sample to a high centrifugal force of 8000 rpm. However, at 10 000 and 12 000 rpm, there was a noticeable broadening of the peak in the intensity distribution (Fig. 4b), along with slight creaming (Fig. S1 in ESI†). The broadening of the peak indicates a polydisperse sample, characterized by the presence of particles of various sizes, as corroborated by the relatively high PDI values for these samples. The formation of larger droplets due to the aggregation of smaller ones results in a more complex size distribution. The gradual broadening of the peak with increasing centrifugal force suggests that the sample is prone to aggregation under high centrifugal stress.

3.3.3 Ionic strength stability. Testing the stability of NE against varied salt concentrations is crucial for pesticide application for various reasons like environmental conditions, effectiveness of pesticide delivery, compatibility with agricultural practices, storage, and transportation. Pesticides are often applied in diverse environmental conditions where the water used for dilution can have varying salt concentrations. Also, agricultural practices often involve mixing pesticides with various fertilizers and other agrochemicals that can contain salts. Stability tests ensure that the NE can be safely mixed without destabilizing.[13] This compatibility is crucial for the practical use of pesticides in integrated pest management systems. However, the introduction of ions can act as a shield, mitigating the electrostatic interactions between droplets and thereby impacting the stability of the NE.[28] Therefore, the stability of the NE was assessed across various salt concentrations. Fig. 4c illustrates HDD, PDI, and intensity variation of different NE droplets. The droplet HDD slightly decreased across samples with salt concentrations ranging from 1 to 15 g L^{-1} (equivalent to 17 to 513 mM). However, a gradual increase in HDD was noted between 30 and 75 g L^{-1} (513 mM to 1.28 M) salt concentrations. This suggests that the electrostatic repulsion between droplets remained strong at relatively low salt concentrations. While our study focused on environmental stresses such as temperature, centrifugal forces, and salt concentration, additional factors like UV exposure, humidity, and pH variations could also influence stability. Future research will aim to incorporate these variables for a more comprehensive evaluation of the NE's environmental resilience. However, at higher salt ion concentrations, the electrostatic repulsion became insufficient to counteract the attractive forces, such as hydrophobic interactions and van der Waals forces. These attractive forces prevailed, leading to increased droplet aggregation and consequently, an increase in particle size. Although no clear correlation was observed with the corresponding PDI

Table 2 Mean diameter and PDI of NE droplets under varied temperature, centrifugal force and salt concentration

Temperature (°C)				
	100	80	60	40
Mean dia	151.5 ± 5.6	151 ± 5.2	153 ± 5	154 ± 4.1
PDI	0.218 ± 0.08	0.208 ± 0.09	0.183 ± 0.08	0.187 ± 0.09

Centrifugation (RPM)					
	12 000	10 000	8000	6000	4000
Mean dia	180.9 ± 5.2	224.1 ± 4.5	208.7 ± 6.3	204.3 ± 5.5	165.1 ± 5.2
PDI	0.276 ± 0.13	0.278 ± 0.1	0.249 ± 0.1	0.247 ± 0.12	0.199 ± 0.08

Salt concentration (g L^{-1})							
	75	60	45	30	15	10	1
Mean dia	1808 ± 5.1	245 ± 5.5	178.3 ± 6.4	168.5 ± 5.7	141.1 ± 5.3	146.6 ± 6.1	147.3 ± 5.2
PDI	0.213 ± 0.11	0.141 ± 0.06	0.158 ± 0.08	0.152 ± 0.08	0.231 ± 0.1	0.222 ± 0.1	0.198 ± 0.09

values, all values were consistently below 0.3. A similar trend was observed in curcumin NE studies, where the addition of NaCl beyond 300 mM led to NE destabilization. This phenomenon can be attributed to the high concentration of NaCl reducing electrostatic repulsion, thereby destabilizing the droplets.[29] In another study conducted by Yan *et al.* (2024),[26] it was observed that the zeta potential value decreased with rising salt concentrations, attributed to the attraction of Cl^- ions diminishing the electrostatic repulsion. Therefore, it can be concluded that the chosen NE formulation had a strong buffering capability over a wide variation in ionic strength. Table 2 sums the variation in mean diameter of NE droplets and PDI under the tested conditions.

3.4 Surface tension analysis

Surface tension plays a critical role in the formation and stability of NEs as well as the spreading of the droplet. Typically, surfactants aid in reducing the surface tension and the interfacial tension which facilitates the emulsification process. The adsorption of surfactant particles at interfaces is closely related to the magnitude of the surface tension. Lower surface tension indicates stronger adsorption of the surfactant particles at the interface, which enhances their stability and effectiveness in reducing surface energy.[28] Moreover, a reduction of surface tension, in turn, lowers the energy required to synthesize the NE. The surface tension was evaluated using the pendant drop method, and the results are outlined in Fig. 5. In a tertiary mixture, as studied here, the neem oil and surfactant can influence the surface tension of the mixture. For comparison, the surface tension of the neem oil–water mixture without any surfactant has been shown in Fig. 5a. As can be observed, the surface tension of the neem oil–water mixture without any surfactant is higher than the corresponding tertiary mixture with the rhamnolipid. Specifically, the addition of rhamnolipid as surfactant has stabilized the NE by reducing the surface tension of the mixture from 43, 44, and 42 to 32, 34, and 35 mN m^{-1}, respectively, for NE with oil (v/v)% of 5, 10, and 15. In the current study, the chosen oil/surfactant (O/S) ratios were all above the critical micellar concentration (CMC), the point of

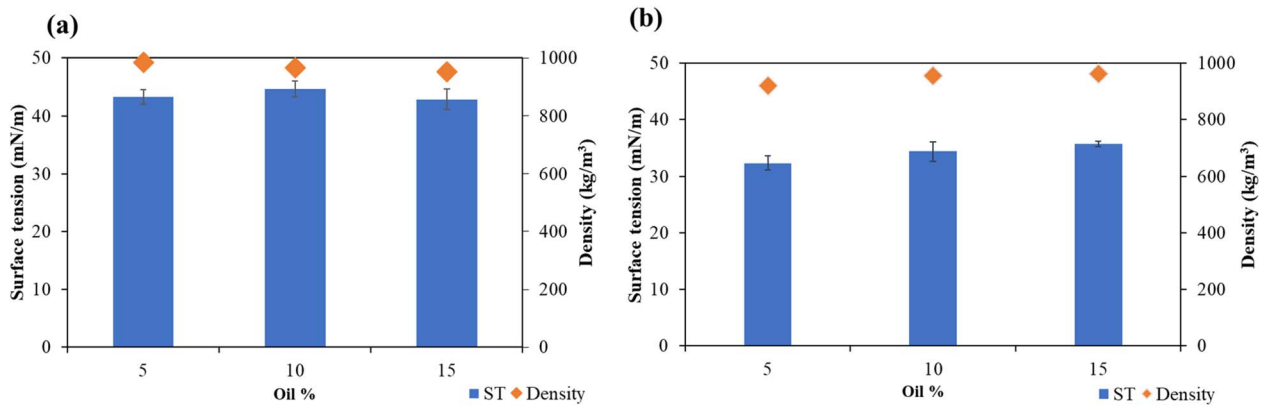

Fig. 5 Surface tension and density of (a) neem oil and water mixture and (b) NE formulations with different oil%.

self-assembly, and therefore, higher or lower O/S ratio is not expected to impact the surface tension values directly. It is to be noted that all the mixtures with or without the rhamnolipid feature lower surface tension than that of pure water (72 mN m^{-1}). Fig. 5b shows a slight increase in surface tension with an increase in oil percentage. The density of neem oil was 789 kg m^{-3}, and all the NE formulations had a density of 920–962 kg m^{-3}. In summary, both the density and surface tension profile do not show much variation over the oil loading, suggesting that rhamnolipid was effective in achieving good dispersion, thereby leading to a consistent density profile.

3.5 Wettability and evolution of contact angle

The CA evolution was evaluated on different surfaces to understand the wetting behavior. Specifically, a lower initial CA coupled with a fast reduction in the CA values (spontaneous droplet spreading) is crucial for increasing the surface coverage and enhancing the activity of the bioactive ingredients present in the droplet. The CA was evaluated for three test surfaces: a smooth glass substrate (minimal surface roughness effects) and two leaves with natural microstructures, hibiscus and rose. The SEM images of the leaf surfaces are shown in Fig. 6, at different magnifications. As can be observed, the two leaf surfaces feature distinct microstructures. Upon comparing similar magnification, it was observed that the roughness features are relatively bigger for the hibiscus leaf than for the rose leaf. Furthermore, a comparison of Fig. 6(1d) and (2d) corresponding to the highest magnification shows that the rose leaf surface consists of further multiscale hierarchical roughness features.

The CA evolution was monitored over 150 seconds for each emulsion component—water, neem oil, and a surfactant solution containing 16.6 g L^{-1} rhamnolipid. This individual component study on each test surface is illustrated in Fig. 7. The leaves featuring the natural roughness exhibited relatively higher CA as compared to the smooth glass slide, with the rose leaf featuring the highest CA among the three test surfaces. A relatively higher CA on the rose leaf can be ascribed to the multiscale roughness along with the smaller roughness features compared to the hibiscus leaf, as observed in Fig. 6. On the smooth glass slide, the CA for water remained fairly stable. However, the CA of both neem oil and surfactant solution declined non-linearly, with a rapid decrease during the first 30 seconds, followed by a slower reduction, indicating progressive dynamic spreading of the liquid. The dynamic spreading behavior is similar to earlier studies on aqueous surfactant solutions.[30] Notably, the lowest final CA was achieved for the surfactant solution on the glass slide. Interestingly, the CA remained stable, and spreading was observed to be minimal for both the hibiscus and rose leaves when neem oil and surfactant solution were used. This starkly contrasts the behavior on a smooth glass slide where spreading was present. Furthermore, the water contact angles on the hibiscus and rose leaves indicate a predominantly hydrophobic nature (CA > 90°), while neem oil and surfactant solution exhibited more philic behavior (CA < 90°) on the leaves. The above indicates that the roughness features on the leaf surface enhance hydrophobicity and can inhibit the spreading of liquid.

Water among the test liquids exhibited the highest average CA, indicating lower wetting. The microstructures on the leaves restrict wetting by the water droplets by forming energy barriers. The surfactant solution and neem oil displayed a more philic behavior and higher wetting. This indicates that the water itself cannot provide enough spreading, while the wetting of the surfactant solution and neem oil with the ability to attain lower CAs indicates their potential as additives to achieve improved wetting.

Following the above analysis, we evaluated the wetting behavior of the emulsion. Specifically, we investigated the effect of the neem oil composition, which is the bio-active ingredient present in the NE formulations, on the wetting behavior of the three test surfaces. Fig. 7g–i shows the temporal evolution of the NE droplet with varying oil concentrations on the test surfaces with corresponding droplet images shown in Fig. 7j–l.

For all the cases, the droplet's CA remains significantly below 90°, indicating a philic interaction, and can be categorized as partial wetting of the surface.[31] Furthermore, for all the

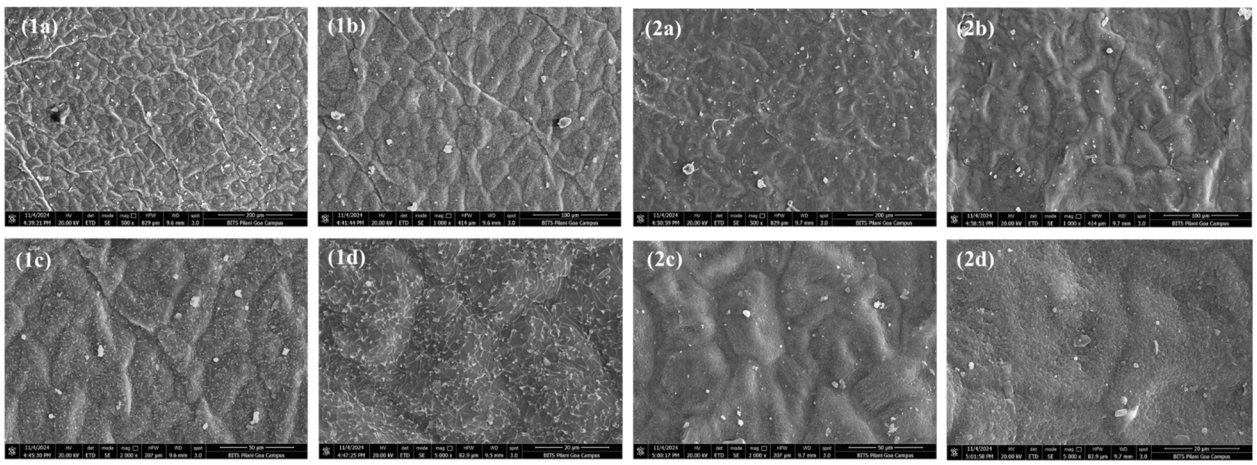

Fig. 6 SEM images of (1) rose and (2) hibiscus leaves as viewed under (a) 500×, (b) 1000×, (c) 2000×, and (d) 5000×.

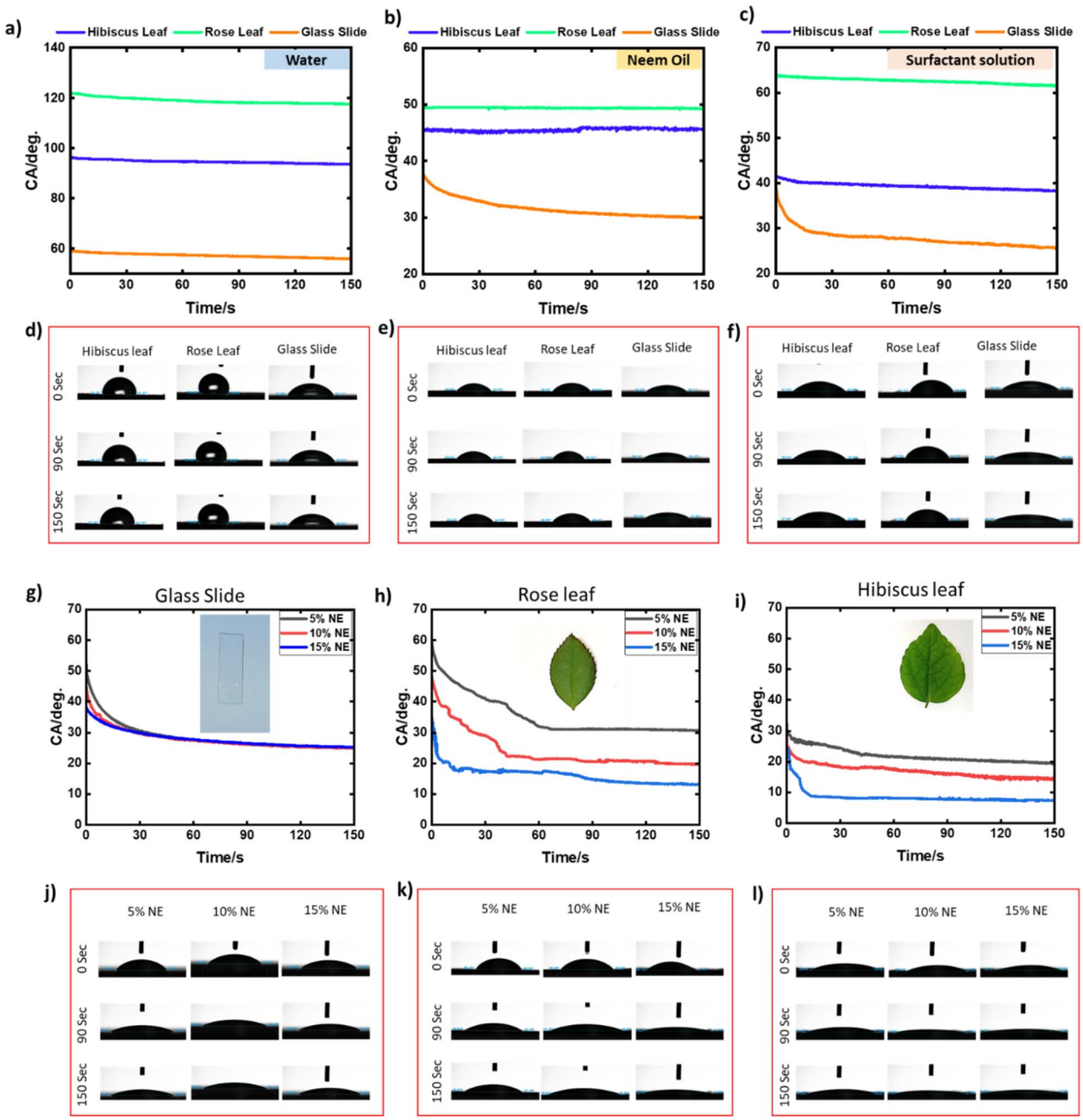

Fig. 7 Evolution of the CA over 150 seconds for (a) water, (b) neem oil, and (c) surfactant solution containing 16.6 g L^{-1} rhamnolipid on three test surfaces: hibiscus leaf, rose leaf, and smooth glass surface. Corresponding droplet images at 0 s, 90 s, and 150 s during the spreading for (d) water, (e) neem oil, and (f) the surfactant solution containing 16.6 g L^{-1} rhamnolipid. Evolution of the CA over 150 seconds for varying oil concentration in the NE for (g) glass slide, (h) rose leaf, and (i) hibiscus leaf. Corresponding droplet images at 0 s, 90 s, and 150 s during the spreading for (j) glass substrate, (k) rose leaf, and (l) hibiscus leaf.

substrates, the CA of the NE gradually reduces with time, indicative of the spontaneous spreading of NE. In Fig. 7g, the NE droplet shows gradual spreading on the glass slide, with a non-linear rapid decrease in CA during the initial phase (0–30 s), following which the rate of CA reduction slowed down. Similar non-linear spreading of emulsion on smooth surfaces has been reported in earlier studies.[32] Interestingly, we observed that the initial CA, corresponding to time $t = 0$, decreased with an increase in the concentration of neem oil in the NE from ~50° for 5% neem oil to ~36° for 15% neem oil. However, after approximately 40 seconds, the temporal evolution of the CA remained consistent, with the final CA values stabilizing at similar values (27°) across all samples by the end of the 150 second experiment.

Following the tests on the smooth glass slide, further wettability studies were conducted on two different leaf surfaces: rose and hibiscus. The evolution of the CA for both leaf surfaces, corresponding to neem oil concentrations ranging

from 5% to 15%, is shown in Fig. 7h and i. The initial CA corresponding to time $t = 0$ was found to be <90° for both the leaves at all neem oil concentrations, indicative of good wetting ability on the leaf surface. Consistent with the observations on the glass slide, the initial CA decreased as the neem oil concentration increased from 5% to 15%. However, the final CA was not found to be the same for varying oil compositions. Instead, distinct final CA values were observed for each neem oil concentration, with lower CA values recorded for higher neem oil content. Furthermore, it was observed that the initial CA (for $t = 0$ s) and the final CA ($t = 150$ s) were higher for the rose leaf than for the hibiscus leaf. Rapid NE spreading results in better surface coverage and higher agrochemical activity. Therefore, a higher neem oil concentration of 15% proves to be a more effective NE formulation, as indicated by its lower final contact angle, faster spreading rate, and quicker stabilization to steady-state values. The wetting behavior of the 15% NE formulation was further tested on horticultural crops such as fenugreek and spinach leaves, where a higher wetting (CA < 90°) with a spontaneous spreading was observed, similar to that obtained for the hibiscus and rose leaves (Fig. S4†).

In agreement with the behavior on the glass slide, the CA decreased with time for all NE compositions on both leaf surfaces, indicative of spontaneous spreading. This is in stark contrast to that observed for the surfactant solution and the neem oil when tested individually on the leaf surface, where negligible spreading was observed. Furthermore, unlike the smooth reduction seen on the glass surface for the NE, the CA reduction on the leaf surfaces was not uniform. This can be attributed to the inherent surface roughness and structural features, such as the veins of the leaves. Overall, the results suggest a synergistic effect when surfactant and neem oil are used together on the leaf surface, along with surface roughness, which collectively promotes higher spreading and a lower CA.

The free energy of the droplet placed on the substrate (Φ) after neglecting the surface forces in the vicinity of the three-phase contact line can be expressed as: $\Phi = \gamma_{lv} \times S + PV + \pi a^2(\gamma_{sl} - \gamma_{sv})$.[33] Here the γ is the interfacial tension, and the subscript lv, sl, and sv represent the liquid–vapor, solid–liquid, and solid–vapor interface; a is the radius of the droplet base; S is the area of the liquid–vapor interface; P is the excess pressure, and V is the liquid volume. Spontaneous spreading occurs when the total excess free energy of the system decreases. Based on the derivatives of the excess free energy with interfacial tension, it was deduced that reduction in the free energy occurs when γ_{lv} decreases and/or γ_{sl} decreases through the adsorption of the surfactant at these interfaces or γ_{sv} increases when the surfactant adsorbs in front of the three-phase contact line.[33] From the spreading coefficient (S_c) perspective also, which is expressed as $S_c = \gamma_{sv} - \gamma_{lv} - \gamma_{sl}$, a decrease in the γ_{lv}, γ_{sl}, and an increase in the γ_{sv} can enhance the spreading.

In general, it has been acknowledged that the spreading behavior of aqueous surfactant solutions involves the adsorption of surfactant molecules at the leading edge of the advancing droplet, specifically at the three-phase contact line comprising the solid–liquid–vapor interface.[31,33,34] Furthermore, the transfer of the surfactant from the droplet interior to the expanding liquid–vapor interface is the rate-determining step at a concentration above CMC.[33,35] We expect that the surfactant adsorption-induced dynamic spreading is the expected mechanism underlying the spreading on the smooth glass surface whenever the surfactant is present, either alone or with the neem oil.

The free energy landscape for a smooth surface comprises a single global energy minimum. In contrast, a rough surface includes multiple local energy minima in addition to the global minimum, with each separated by energy barriers.[36,37] For the smooth glass surface, we can assume that these local minima are separated by very low energy barriers, allowing it to be approximated as having a single global energy minimum. In contrast to the smooth glass surface, the roughness features on the leaves introduce multiple free energy minima and energy barriers for droplet shape change compared to the ideal smooth surface with single global energy minima. The droplet shape stabilizes when the droplet shape is trapped in any of the energy minima. When a droplet with only the surfactant is placed on the rough surface, the change in the free energy landscape resulting from the surfactant adsorption alone is insufficient to overcome the energy barriers posed by the roughness features on the leaf, resulting in significantly lower wetting and spreading. Similarly, when present alone, oil does not spread significantly on the rough leaf surface due to the energy barriers posed by the roughness features. However, when both surfactant and oil are present together, a synergistic effect enables enhanced spreading—a phenomenon likely arising from the combination of surfactant absorption and the effect of oil on the solid–liquid interface. The underlying mechanism is deduced by imaging the area underneath the NE droplet placed on a glass surface under the microscope, shown in Fig. S3 (please refer to ESI†) at different magnifications. Microscopic images revealed that some larger oil droplets were immobile, which are deposited at the base of the glass slide, whereas the smaller droplets remained mobile and suspended in the aqueous phase. At 15% neem oil concentration, crowding of emulsion droplets was observed, obscuring any deposited oil droplets on the glass slide. However, we expect the deposition of the oil droplets to occur nevertheless. While the above is observed for the glass due to the transparency, a similar phenomenon is expected on rough leaf surfaces. We theorize that the deposition of the oil droplets at the solid–liquid interface is the underlying reason for the enhanced spreading and wetting by the NE. When oil droplets are deposited onto the solid–liquid interface, they replace the water molecules in contact with the solid surface, replacing the solid–water interface with the solid–oil interface, causing a reduction in the effective γ_{sl}. The change in the interfacial tension causes additional changes in the free energy landscape beyond what is caused only by the surfactant adsorption mechanism. This additional change in the free energy allows the droplet to overcome the energy barriers for the droplet present on the rough surface, causing enhanced spreading. From the perspective of the spreading coefficient (S_c), such oil droplet deposition is expected to reduce the γ_{sl} further, thereby increasing the spreading coefficient and facilitating spreading.

With increasing neem oil concentration, more oil droplets adhere to the solid surface, progressively leading to a higher change in the solid–liquid interface and the resulting γ_{sl}. These results in a lower CA observed at higher neem oil concentrations. The deposition of oil droplets on the solid surface is time-dependent, with larger oil droplets initially depositing after the NE droplet is placed on the surface. Following this initial phase, further oil droplet deposition on the surface gradually decreases. This is also evident in the spreading behavior on the leaves, where the majority of the spreading is observed only during the initial stages, and the droplet CA reduction is lower in the later stages. While surfactant adsorption alone leads to an insufficient change in the free energy landscape and overcomes the energy barriers to spreading, the combined effect with the oil droplet deposition at the solid–liquid interface further reshapes the free energy landscape enough to enable dynamic spreading.

4 Conclusion and future perspectives

The current study highlights the potential of neem oil-based NE formulations for pesticidal applications, emphasizing the benefits of a carefully optimized composition. The selected NE formulation achieved a higher concentration of active neem oil, displaying enhanced stability and improved wetting performance. By utilizing green ingredients, this formulation offers an environmentally friendly alternative that reduces pesticide resistance and minimizes health risks to farmers. Future research could explore the incorporation of multiple active ingredients or adjuvants, which may broaden the spectrum of pest control and further boost efficacy. Notably, the optimized 15% neem oil formulation demonstrated superior wettability on leaf surfaces, as indicated by a significant reduction in contact angle during dynamic analysis. This study reveals a synergistic effect of neem oil and rhamnolipid in achieving faster wetting compared to their individual use, suggesting a promising direction for future work in NE synthesis and applications.

Consent for publication

All authors read and agreed to submit the manuscript.

Data availability

The data supporting this article have been included as part of the ESI.†

Author contributions

Jayita Chopra – designing and performing experiments, writing the paper, reviewing and editing. Priyanka Sahoo – investigation, formal analysis, reviewing and editing Pradeep K. Sow – writing, formal analysis, validation, Vivek R. – conceptualization, supervision. All the authors read and approved the final manuscript.

Conflicts of interest

There are no conflicts to declare.

Acknowledgements

This research did not receive any specific grant from funding agencies in the public, commercial, or not-for-profit sectors. Our sincere appreciation goes to the Central Sophisticated Instrumentation Facility (CSIF) at BITS Pilani, K K Birla Goa Campus, for providing access to the DLS and SEM facilities.

References

1 R. Gupta, P. Malik, R. Rani, R. Solanki, R. Kumar, V. Malik and T. Kumar, *Plant Nano Biol.*, 2024, **8**, 100073.
2 J. Feng, Q. Zhang, Q. Liu, Z. Zhu, D. J. McClements and S. M. Jafari, *Application of Nanoemulsions in Formulation of Pesticides*, Elsevier Inc., 2018.
3 R. D. Singh, S. Kapila, N. G. Ganesan and V. Rangarajan, *J. Surfactants Deterg.*, 2022, **25**, 303–319.
4 D. S. Bernardi, T. A. Pereira, N. R. Maciel, J. Bortoloto, G. S. Viera, G. C. Oliveira and P. A. Rocha-Filho, *J. Nanobiotechnol.*, 2011, **9**, 1–9.
5 Y. Guo, X. Zhang, X. Wang, L. Zhang, Z. Xu and D. Sun, *Langmuir*, 2024, **40**, 1364–1372.
6 J. F. Masiero, M. C. Knirsch, T. Barreto, G. J. Arantes, M. A. Stephano, K. Ishida, R. Lobënberg and N. A. Bou-Chacra, *Ind. Crops Prod.*, 2024, **208**, 117853.
7 N. G. Ganesan, R. D. Singh, D. Dwivedi and V. Rangarajan, *J. Cleaner Prod.*, 2023, **400**, 136735.
8 A. Wittgens, F. Kovacic, M. M. Müller, M. Gerlitzki, B. Santiago-Schübel, D. Hofmann, T. Tiso, L. M. Blank, M. Henkel, R. Hausmann, C. Syldatk, S. Wilhelm and F. Rosenau, *Appl. Microbiol. Biotechnol.*, 2017, **101**, 2865–2878.
9 L. Bai and D. J. McClements, *J. Colloid Interface Sci.*, 2016, **479**, 71–79.
10 P. Thakur, N. K. Saini, V. K. Thakur, V. K. Gupta, R. V. Saini and A. K. Saini, *Microb. Cell Fact.*, 2021, **20**, 1–15.
11 M. A. Díaz De Rienzo, I. D. Kamalanathan and P. J. Martin, *Process Biochem.*, 2016, **51**, 820–827.
12 L. Pavoni, G. Benelli, F. Maggi and G. Bonacucina, in *Nano-Biopesticides Today and Future Perspectives*, ed. O. Koul, Academic Press, 2019, pp. 133–160.
13 I. F. Mustafa and M. Z. Hussein, *Nanomaterials*, 2020, **10**, 1–26.
14 J. Jerobin, R. S. Sureshkumar, C. H. Anjali, A. Mukherjee and N. Chandrasekaran, *Carbohydr. Polym.*, 2012, **90**, 1750–1756.
15 M. Choupanian, D. Omar, M. Basri and N. Asib, *J. Pestic. Sci.*, 2017, **42**, 158–165.
16 N. Iqbal, D. K. Hazra, A. Purkait, A. Agrawal and J. Kumar, *Colloids Surf., B*, 2022, **209**, 112176.
17 A. T. H. Mossa, R. I. Mohamed and S. M. M. Mohafrash, *Biocatal. Agric. Biotechnol.*, 2022, **46**, 102541.
18 A. Lewińska, *Processes*, 2021, **9**(7), 1180.

19 T. B. Schreiner, A. Santamaria-Echart, A. Ribeiro, A. M. Peres, M. M. Dias, S. P. Pinho and M. F. Barreiro, *Molecules*, 2019, **25**(7), 1538.
20 J. Carpenter and V. K. Saharan, *Ultrason. Sonochem.*, 2017, **35**, 422–430.
21 D. Debraj, J. Carpenter and A. K. Vatti, *Ind. Eng. Chem. Res.*, 2023, **62**, 16766–16776.
22 Y. Zhao, F. Peng and Y. Ke, *RSC Adv.*, 2021, **11**, 1952–1959.
23 K. Gurpret and S. K. Singh, *Indian J. Pharm. Sci.*, 2018, **80**, 781–789.
24 S. M. Dordević, N. D. Cekić, M. M. Savić, T. M. Isailović, D. V. Randelović, B. D. Marković, S. R. Savić, T. T. Stamenić, R. Daniels and S. D. Savić, *Int. J. Pharm.*, 2015, **493**, 40–54.
25 S. Da Costa, M. Basri, N. Shamsudin and H. Basri, *J. Chem.*, 2014, **1**, 748680.
26 Z. Yan, X. Wang, P. Zhao, Y. He, X. Meng and B. Liu, *Food Chem.*, 2024, **441**, 138289.
27 B. Iskandar, H. C. Mei, T. W. Liu, H. M. Lin and C. K. Lee, *Colloids Surf., B*, 2024, **234**, 113692.
28 L. Bai, S. Geng, Y. Zhou, H. Ma and B. Liu, *Ultrason. Sonochem.*, 2024, **104**, 106807.
29 I. Dammak and P. J. do A. Sobral, *Food Biosci.*, 2021, **43**, 101335.
30 N. A. Ivanova and V. M. Starov, *Curr. Opin. Colloid Interface Sci.*, 2011, **16**, 285–291.
31 K. S. Lee, N. Ivanova, V. M. Starov, N. Hilal and V. Dutschk, *Adv. Colloid Interface Sci.*, 2008, **144**, 54–65.
32 Z. Du, C. Wang, X. Tai, G. Wang and X. Liu, *ACS Sustain. Chem. Eng.*, 2016, **4**, 983–991.
33 V. Starov, N. Ivanova and R. G. Rubio, *Adv. Colloid Interface Sci.*, 2010, **161**, 153–162.
34 V. M. Starov, S. R. Kosvintsev and M. G. Velarde, *J. Colloid Interface Sci.*, 2000, **227**, 185–190.
35 M. Von Bahr, F. Tiberg and V. Yaminsky, *Colloids Surf., A*, 2001, **193**, 85–96.
36 C. H. Kung, P. K. Sow, B. Zahiri and W. Mérida, *Adv. Mater. Interfaces*, 2019, **6**, 1–27.
37 T. Huhtamäki, X. Tian, J. T. Korhonen and R. H. A. Ras, *Nat. Protoc.*, 2018, **13**, 1521–1538.